Bioelectrochemistry 119 (2018) 1–9

Contents lists available at ScienceDirect

Bioelectrochemistry

journal homepage: www.elsevier.com/locate/bioelechem

# Immobilization of methotrexate anticancer drug onto the graphene surface and interaction with calf thymus DNA and 4T1 cancer cells

Reza Karimi Shervedani [a,*], Hadiseh Mirhosseini [a], Marzieh Samiei Foroushani [a], Mostafa Torabi [a], Fatemeh Rahnemaye Rahsepar [a], Leila Norouzi-Barough [b]

[a] Department of Chemistry, University of Isfahan, Isfahan 81746-73441, Iran
[b] Department of Genetics and Molecular Biology, School of Medicine, Isfahan University of Medical Sciences, Isfahan, Iran

ARTICLE INFO

*Article history:*
Received 6 March 2017
Received in revised form 13 August 2017
Accepted 15 August 2017
Available online 18 August 2017

*Keywords:*
Immobilization
Methotrexate
Calf-thymus DNA
Graphene
Anticancer drug

ABSTRACT

Immobilization of *methotrexate* (MTX) *anticancer drug* onto the graphene surface is reported through three methods, including either covalent linkage via (a) EDC/NHS organic activators and (b) electrografting of MTX diazonium salt, or (c) noncovalent bonding, resulting in three different *systems*. To evaluate the interaction ability of the immobilized MTX with biological species, calf thymus DNA (ctDNA), mouse 4T1 breast tumor, and *Human foreskin fibroblast* (*hFF*) *cells* as models of the primary intracellular target of anticancer drugs, cancer and normal cells, respectively, are examined. The features of the constructed *systems* and their interactions with ctDNA are followed by surface analysis techniques and electrochemical methods. The results indicate that (i) the amount of the immobilized MTX on the graphene surface is affected by type of the immobilization method; and a maximum value of ($\Gamma = 9.3 \pm 0.9$ pmol cm$^{-2}$) is found via electrografting method, (ii) graphene-modified-MTX has high affinity for ctDNA in a wide dynamic range of concentrations, and (iii) the nature of the interaction is of electrostatic and/or hydrogen bonding type, formed most probably between O—H, N—H and C═O groups of MTX and different DNA functions. Finally, electrochemical impedance spectroscopy results approved the high affinity of the systems for 4T1 cancer cells.



## 1. Introduction

Immobilization of chemical and biological *systems* on the solid surfaces allows excellent control over their behavior and properties, compared with their corresponding behavior in the solution phase [1–3]. Among several studied systems, the therapeutic and anticancer drugs are especially important [4–7]. The components of *immobilized systems* play important roles to improve the behavior and characteristics of the *system*; such as contrasts in imaging and diagnosis, selectivity in drug delivery, and sustain and release efficiency, therapeutic dose and adverse effects of the drug [4,5,8–11].

To date, numerous biological studies have demonstrated that DNA is the primary intracellular target of anticancer drugs [12,13]. Interaction between anticancer drug and DNA can cause damage in cancer cells; the drug blocks division and results in death of the cells [14–16]. This interaction has been studied by different methods, including spectroscopy [17–19] and electrochemistry [20–23].

Methotrexate (MTX), as an anticancer drug, can influence on DNA replication and cell proliferation via integrating within the spaces between two adjacent base pairs of DNA [24]. However, the MTX performance is limited by its low solubility, dose-related toxicity, lack of selectivity, rapid diffusion throughout the body, short half-life in bloodstream, and drug resistance by target cells [25]. Therefore, MTX has been attached onto different nanocarriers to improve its pharmacological properties [26–29].

Graphene has been widely used as the supports in science and technology [30,31], particularly as the carriers for targeted drug delivery [32–34].

Interaction of DNA with MTX, based on the DNA modified surface, has been investigated by electrochemical methods to determine the MTX concentrations in the solution phase [35–38]. Also, attachment of MTX onto graphene in aqueous solution has been investigated by using spectroscopic methods [39]. However, there is a lack of information regarding the electrochemical behavior of graphene-MTX confined on the surface; especially, to our knowledge; no attention has been paid to study the interaction between the graphene-MTX modified electrodes with single- and double-strand DNA (ss-DNA and ds-DNA). The immobilization of MTX onto a suitable modified surface allows obtaining valuable information about its confined redox reaction and surface behavior, which in turn, helps to follow its interaction with DNA *as a primary intracellular target of anticancer drugs, mouse 4T1 breast tumor, as a model of cancer cells, and Human foreskin fibroblast* (*hFF*) *cells as a model of normal cells* [40].

* Corresponding author.
*E-mail address:* rkarimi@sci.ui.ac.ir (R. Karimi Shervedani).

http://dx.doi.org/10.1016/j.bioelechem.2017.08.004
1567-5394/

Accordingly, the present work is intended to perform a systematic comparative investigation between the behavior of *systems* formed from MTX immobilized on graphene (graphene nanosheets, GNs, and graphene oxide, GO) surface via three different methods, including either covalent linkage via (a) EDC/NHS organic activators and (b) electrografting of MTX diazonium salt, or (c) noncovalent bonding, abbreviated, respectively as GO-MTX(E/N), GNs-MTX(ER) and GO/MTX. Finally, interaction of the constructed systems with calf thymus DNA (ctDNA) and 4T1 cancer cells is studied.

## 2. Methods and materials

### 2.1. Materials and reagents

Graphite powder (1–2 μm, Aldrich), Methotrexate (MTX): ((2*S*)-2-[(4-{[(2,4-Diaminopteridin-6-yl)methyl](methyl)amino}benzoyl)amino]pentanedioic acid, double-strand calf thymus DNA (ds-ctDNA), 1-ethyl-3(3-dimethylamino)-propyl) carbodiimide (EDC), *n*-hydroxysuccinimide (NHS), and other chemicals were of analytical grade obtained from commercial sources (Sigma-Aldrich® or Merck®). All solutions were prepared with distilled water. The test solutions were deaerated with high purity argon gas for 10 min before each experiment and blanketed with the gas during the experiments. Phosphate buffer solution (PBS) was prepared by mixing 0.1 M $KH_2PO_4$/0.1 M $K_2HPO_4$ and the required pH was adjusted by 0.1 M $H_3PO_4$ or 0.1 M NaOH. The solution was placed in an autoclave under 100 °C for 1 h to *sterile*; then, it was cooled and stored at 4 °C. The MTX solutions were prepared daily by dissolution of required amounts of MTX in 0.1 mM NaOH. Dilute solutions of ds-ctDNA were prepared immediately before using from a stock solution of $6.0 \times 10^{-3}$ M, prepared by dissolution of ds-ctDNA in PBS, pH 7.0.

Decomposition of ds-ctDNA into single strands was carried out by heating a solution of ds-ctDNA at 100 °C. Then, the sample was rapidly cooled in ice-cold water and used for measurement immediately [41].

The mouse 4T1 breast cancer cells samples were cultured in Dulbecco's Modified Eagle Medium supplemented with 10% fetal bovine serum, penicillin (50 U/mL) and streptomycin (50 μg/mL). The hFF cells were cultured under the same conditions, except a high concentration of glucose was used in the culture medium.

### 2.2. Immobilization of MTX onto the GC surface

The GO was synthesized according to the Hummers' method [42] partially modified by us [43]. Also, several sets of clean GC electrodes were prepared [43,44] and modified through three methods including either *covalent attachment* via (a) EDC/NHS organic activators and (b) electrografting of MTX diazonium salt, or (c) *noncovalent bonding* to construct the working electrodes, abbreviated, respectively, as GC-GNs-MTX(E/N), GC-GNs-MTX(ER) and GC-GNs/MTX (see Supplementary Data, Section 1 and Figs. S1 to S3).

### 2.3. Interaction of ctDNA with MTX-modified GC-GNs electrodes

Three sets of each modified electrode; (a) GC-GNs-MTX(E/N), (b) GC-GNs-MTX(ER), and (c) GC-GNs/MTX were prepared, and further modified with ctDNA. Accordingly, a 10.0 μL of $1.0 \times 10^{-9}$ M ss-ctDNA or ds-ctDNA solutions were individually superposed on the topside of each above-mentioned modified electrode and allowed at least for 15 min, in order to complete interaction between the immobilized MTX and ctDNAs. Therefore, we had two sets of each electrode modified with ss-ctDNA and ds-ctDNA and one set as blank respect to ctDNA, for studying. The modified electrodes were washed with distilled water to remove loosely adsorbed species, and then used for measurements.

For AFM measurements, screen-printed carbon electrodes (SPCE; model DS110, DropSens S.L., Oviedo, Spain) were used as a platform, and modified according to the method explained for the GC electrode.

### 2.4. Interaction of 4T1 cells with MTX-modified GC-GNs electrodes

The affinity of MTX immobilized on GC-GNs electrode surface toward cancer cells was investigated using mouse 4T1 breast tumor as a model. The electrodes were washed thoroughly with the sterile PBS and immersed separately into the sterile solutions, PBS pH 7.4, containing $10^5$ cells/mL 4T1 for 30 min. Then, the electrodes were removed, washed thoroughly with the sterile PBS, and used for electrochemical impedance spectroscopy (EIS) measurements.

### 2.5. Apparatus and physicochemical characterization

Topography and structural properties of the electrode surfaces were studied by using Atomic Force Microscopy (AFM) method in noncontact mode by using DME model C26, Dualscope™ Denmark. The AFM images were analyzed by using DualScope SPM 2.4.2.1 software. The FESEM images were acquired by using a scanning electron microscope, Hitachi S4160, Cold Field Emission, Japan. The ATR-FTIR spectra of the surface were obtained in the wavenumber range of 600 to 4000 $cm^{-1}$ by using Bruker Tensor 27 spectrometer, equipped with a CsI crystal, Pike Technologies. The UV–Vis measurements were performed by using UV–Vis-NIR spectrophotometer Cary 500.

The electrochemical measurements were performed on Potentiostat/Galvanostat Autolab30 in a conventional three-electrode glass cell, using the modified GC disk electrode as working, a piece of Pt with a large surface area as counter electrode, and the SCE as reference electrode. All experiments were performed at room temperature and under argon atmosphere.

## 3. Results and discussion

The constructed composite systems and their interaction with ctDNA (Supplementary Data, Section 1) are characterized by electrochemical methods as CV and DPV, and surface analysis techniques as ATR-FTIR, AFM, FESEM and UV–Vis. Finally, the affinity of MTX immobilized on GC-GNs electrode surface toward a mouse 4T1 breast tumor as a model is investigated.

### 3.1. Characterization by electrochemical methods

#### 3.1.1. Immobilization of MTX

Since MTX is electroactive [45] (Scheme 1), modification of GC surface could be followed based on the redox faradaic currents of immobilized MTX. The method is effective and preferred when it is possible [2], compared with that is based on using external redox reaction. The DPVs obtained in the absence of any external redox probe on GC-GNs-MTX(E/N) (A), GC-GNs-MTX(ER) (B), and GC-GNs/MTX (C) in comparison with blank GC (a′) and GC-GNs (b′) electrodes are presented in Fig. 1. While no significant faradaic current is observed for voltammograms recorded on GC and GC-GNs electrodes (Fig. 1, Panel Blank, curves a′ and b′), a well-defined voltammetric faradaic wave (curves a to c) is observed around $E_{1/2} = (-0.74 \pm 0.05)$ V for electrodes (A)

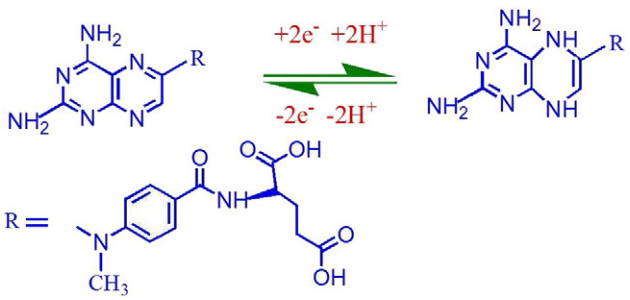


**Scheme 1.** Schematic illustration for proposed redox mechanism of MTX.

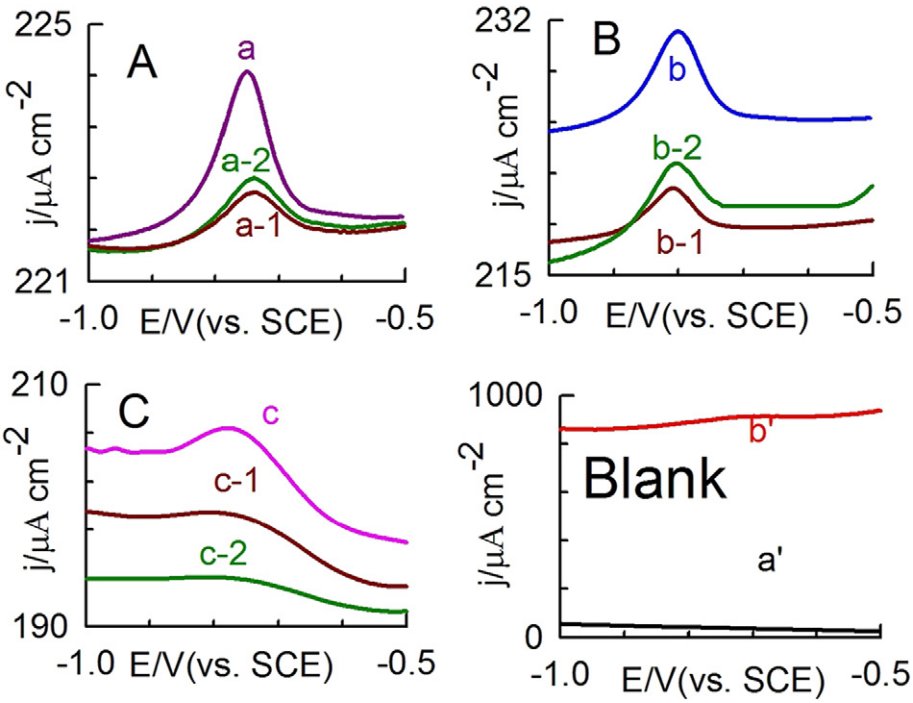


**Fig. 1.** The DPVs recorded in 0.1 M PBS, pH 7.0, *in the absence of any external redox probe on* (A) GC-GNs-MTX(E/N), (B) GC-GNs-MTX(ER), and (C) GC-GNs/MTX electrodes. The notations (a), (b) and (c) are referred to "before accumulation of ctDNAs", and those labeled with numbers (a-, b-, and c-1 and 2) are referred to "after accumulation of ctDNAs" from $1.0 \times 10^{-9}$ M ss-ctDNA or ds-ctDNA solution, in PBS, pH 7.0, 15 min, respectively.

to (C), which is attributed to the redox reaction of immobilized MTX (Scheme 1). The surface coverage of MTX ($\Gamma = 2.4 \pm 0.2$, $9.3 \pm 0.9$ and $8.85 \pm 1.54$ pmol $cm^{-2}$ obtained by related voltammetric reduction charges) can be used to show the *relative* amount of immobilized MTX, accordingly, the following order is observed here: (B) ≥ (C) ≫ (A), implying that case A is not efficient for accumulation of MTX, probably due to competitive hydrolysis [46].

*3.1.2. Interaction with DNA*

Interaction study of DNA with various molecules, including anticancer drugs, is interesting, due to several important biomedical applications, especially drug delivery systems, and has been reported by several papers [13,16,20,22]. Understanding DNA interaction patterns can speed up drug discovery, development, and delivery processes [47].

Fig. 1A to C (curves a-, b-, c-1 and 2) show a decrease in the faradaic peak currents of MTX upon incubation of the modified electrodes into ss-ctDNA or ds-ctDNA solutions, implying the accumulation of DNAs on the surface. The observed results are in good agreement with those reported for interaction of anticancer drugs-DNA in the solution phase [16,22]. The decreases observed in the peak current of MTX upon addition of ctDNA onto the MTX modified surfaces can be explained based on decrease in the equilibrium concentration of free MTX on the surface. MTX and ctDNA are supposed to form an electrochemically inactive MTX–ctDNA complex that cannot perform a redox reaction at the electrode surface [22].

*3.1.3. Analytical response*

To show that the interaction between MTX-modified surfaces with ctDNA can take place in a wide range of ctDNA concentrations, the DPVs are recorded on GC-GNs-MTX(ER) electrode, before and after accumulation of ss-ctDNA or ds-ctDNA from separate solutions containing different concentrations of them (Supplementary Data, Fig. S4).

In addition, while the structures formed via *methods b* and *c* are both reproducible and benefit of high loading, the GC-GNs-MTX(ER) structure formed via C—C electrografting [43] of MTX diazonium salt (*method b*) is highly stable, thus, it is more appropriate for sensing intentions. Alternatively, the GC-GNs/MTX structure formed via electrostatic interaction between GC-GNs and MTX (*method c*) is sensitive to the pH and ionic strength (μ) of the solution, thus, it is more appropriate for drug delivery intentions. It is clear that the strength of electrostatic interactions is dependent on pH and μ, allowing to release the MTX drug by adjusting the solution conditions (still, the system formed via *method a* is not highly efficient, see Section 3.1.1).

Variations of the MTX reduction peak current of GC-GNs-MTX(ER) electrode, measured vs. ss-ctDNA or ds-ctDNA concentration in the accumulation solution, shows a wide dynamic response range (Supplementary Data, Fig. S4, Insets). Since the peak current of immobilized MTX is varied linearly with DNA concentration in accumulation solution, the modified surface is promising for fabrication of DNA biosensors where no significant modification performs on DNA strands [48]. A detailed study of this behavior is interesting as a new challenge for DNA sensing; however, it has not been intended in the current work.

*3.1.4. Nature of the interaction between ctDNAs and the immobilized MTX*

(i) *DPV*; Interactions between small molecules and DNA double helix can be categorized into three models; (i) intercalative, (ii) groove, and (iii) electrostatic bindings [16,22]. Intercalative and groove binding models are dependent on DNA structure so that the chance of interaction via these two models decreases for denatured (single strand) DNA. Since the current results show that the interactions of immobilized MTX continue to operate even with ss-ctDNA (Fig. 1A to C, curves a-, b-, c-1 and 2), the nature of interactions between MTX and DNAs can be a type of *electrostatic binding*.

(ii) UV–Vis; The nature of interaction between MTX and ctDNA is also verified by recording UV–Vis absorption spectra of GO/MTX suspension solution and its mixture with ss-ctDNA or ds-ctDNA (Fig. 2A) as follows [16,22]:

The suspension solution of GO shows an absorption peak around 240 nm corresponding to the π-π* transitions of aromatic C—C bonds (Fig. 2A, curve a) [49]. In addition, MTX has shown three characteristic bands in solution phase, around 260, 300 and 370 nm (Fig. 2B). After adsorption of MTX on GO surface (Supplementary Data, Section 1), a broad

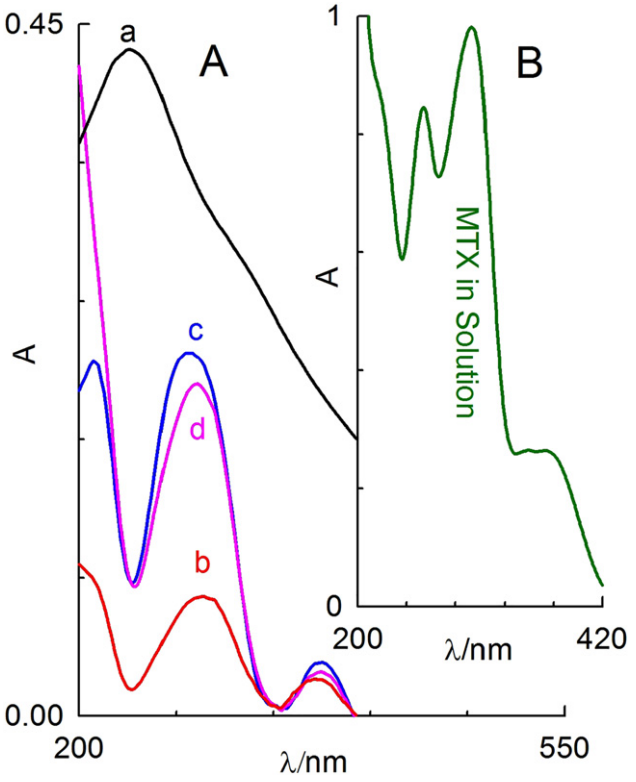


**Fig. 2.** (A) UV–Vis spectra obtained from 0.6 mg $mL^{-1}$ separate solutions of (a) GO, (b) GO/MTX, (c) GO/MTX containing 1.0 × $10^{-9}$ M ss-ctDNA, and (d) GO/MTX containing 1.0 × $10^{-9}$ M ds-ctDNA. (B) UV–Vis spectrum of 50.0 μM of MTX solution.

peak is formed around 290 nm (Fig. 2A, curve b) which can be due to overlapping the 240 nm GO peak with the 260 and 300 nm MTX peaks (Fig. 2B). Notably, the change observed in the UV–Vis spectrum supports loading of MTX on GO surface. Finally, by addition of ss-ctDNA or ds-ctDNA into the GO/MTX solution, the absorbance intensities are increased considerably at 290 nm and slightly at 370 nm without any shift in the peak energies (Fig. 2A, curves c and d). Since no red shift has been observed in this process, the nature of the interaction between MTX and ctDNAs can be a type of *electrostatic binding* [16,22].

### 3.2. Characterization of the systems by surface analysis techniques

#### 3.2.1. Characterization by ATR-FTIR

The ATR–FTIR spectroscopy measurements (Fig. 3) are performed in conjunction with electrochemical measurements (Fig. 1) to support step-by-step attachment of GNs, MTX, ss-ctDNA or ds-ctDNA layers onto the GC electrode surface through noncovalent and electrografting of MTX diazonium salt (please note that GC-GNs-MTX(E/N) system, as discussed in Section 3.1.1, did not show a good efficiency, thus, it is not studied further from here).

While the spectrum of GNs-GC surface (Fig. 3B) shows three significant peaks around 1622, 1740 and 3400 $cm^{-1}$ [44], attributed to the stretching vibrations of C═C, C═O and O—H, respectively, the spectrum of GC surface (Fig. 3A) is nearly featureless with two peaks around ~3600 and 3700 $cm^{-1}$, attributed to the stretching and bending modes of gas phase $H_2O$ molecular clusters.

The vibrational spectrum obtained on GC-GNs-MTX(ER) (Fig. 3B) consists of C═O stretching peak around 1638 $cm^{-1}$, the band caused by combination of C—N stretching and N—H rocking character at 1317–1390 $cm^{-1}$, C—O stretching at 1210–1320 $cm^{-1}$, C—N stretching at 1000–1160 $cm^{-1}$, aliphatic C—H stretching at 2982 $cm^{-1}$, and O—H

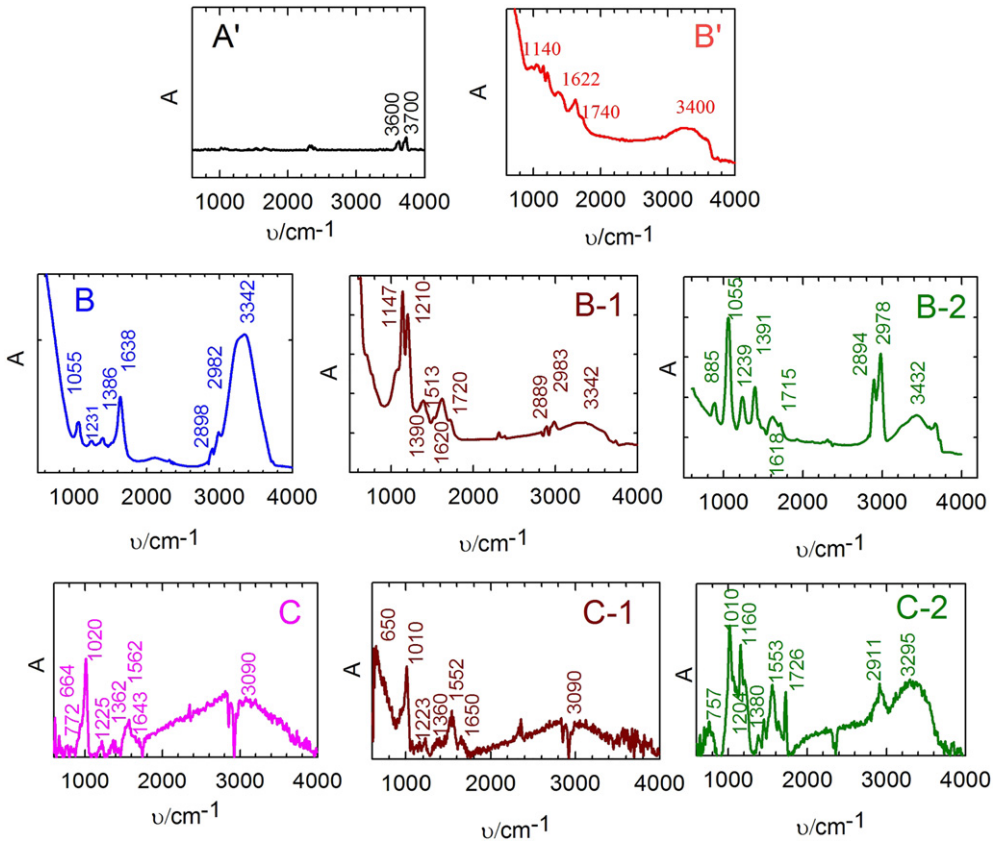


**Fig. 3.** ATR–FTIR spectra obtained on (A′) GC, (B′) GC-GNs, (B) GC-GNs-MTX(ER), (B-1) GC-GNs-MTX(ER)-ss-ctDNA, (B-2) GC-GNs-MTX(ER)-ds-ctDNA, (C) GC-GNs/MTX, (C-1) GC-GNs/MTX-ss-ctDNA, and (C-2) GC-GNs/MTX-ds-ctDNA electrode surfaces.

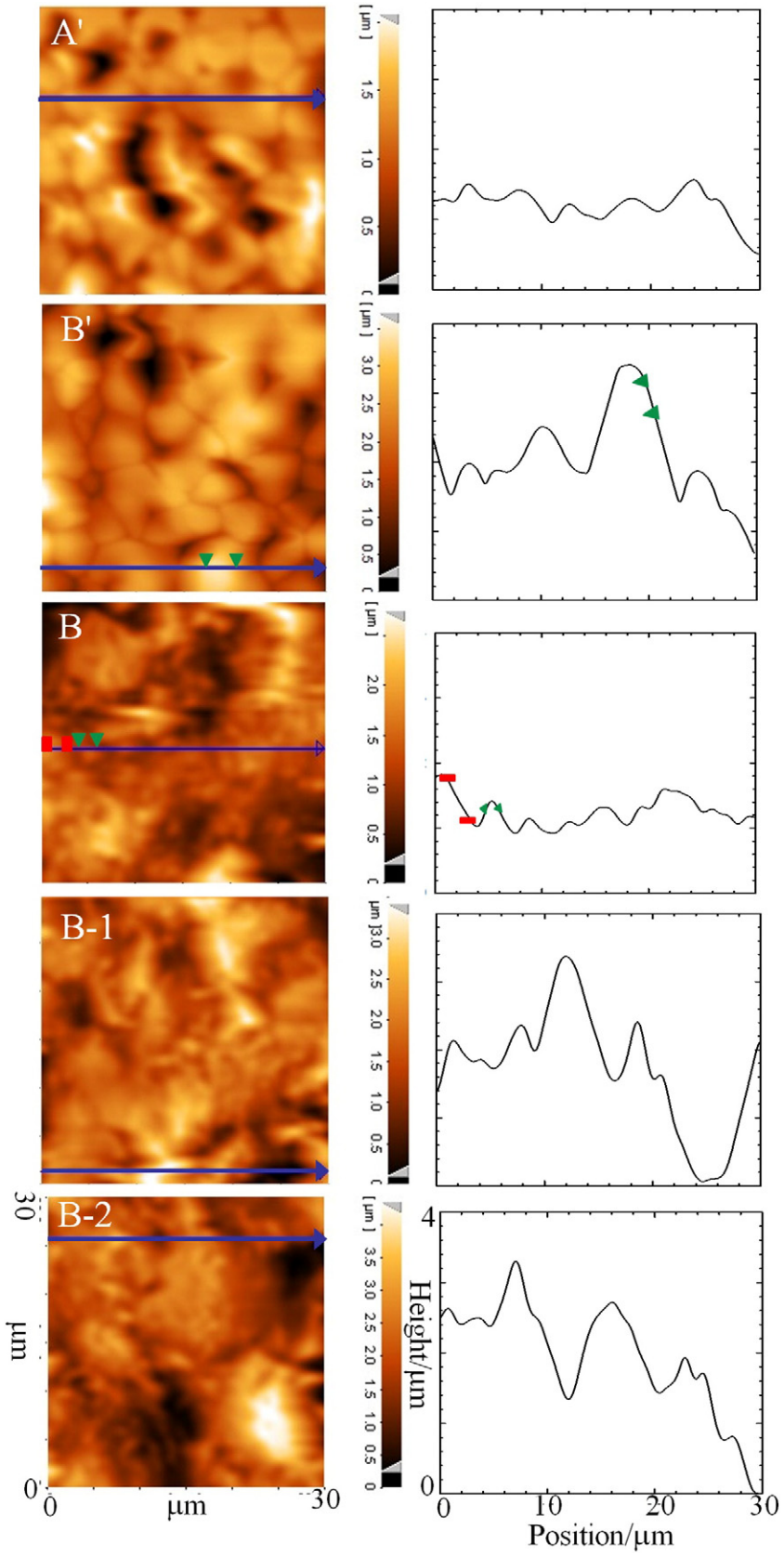


**Fig. 4.** AFM images and the corresponding line profiles obtained on (A′) SPCE, (B′) SPCE-GNs, (B) SPCE-GNs-MTX(ER), (B-1) SPCE-GNs-MTX(ER)-ss-ctDNA, and (B-2) SPCE-GNs-MTX(ER)-ds-ctDNA electrodes. Green triangle and red square markers, respectively, indicate the size of GNs and MTX.

stretching around 3342 $cm^{-1}$ [50]. The ATR-FTIR spectra investigation of ss-ctDNA and ds-ctDNA attached on GC-GNs-MTX(ER) surface (Fig. 3B-1 and 2) revealed the following effects. (1) The intensity of peaks O—H and C═O (Fig. 3B) is decreased significantly (Fig. 3B-1 and 2), which provides evidence for the interaction of MTX via its O—H and C═O groups with DNA. (2) The new absorption band appeared around ~1720 $cm^{-1}$ provides good evidence for interaction of MTX with phosphate groups of ctDNA via formation of hydrogen bond and/or electrostatic interaction. These results are in agreement with those reported for interaction of DNA with anticancer drugs in the solution phase [35,51].

Noncovalent immobilization of MTX on GC-GNs surface causes some changes in the main vibrational frequencies of MTX functional groups, and also, the appearance new bands in the ranges of ~630–750 $cm^{-1}$ and 1490–1600 $cm^{-1}$ (Fig. 3C), which can be attributed to the wagging and bending vibrations of N—H, respectively. The spectral changes observed upon attachment of ss-ctDNA or ds-ctDNA molecules on GC-GNs/MTX electrode (Fig. 3C-1 and 2) include a decrease in the absorption frequency of C—O, C═O and N—H vibrations of MTX. The shift of all these bands is evidence that interaction between MTX and ctDNA occurs mainly through these functional groups [38].

Overall, the ATR-FTIR results strongly support aforementioned electrochemical findings regarding effective interaction of modified surfaces, GC-GNs-MTX(ER) and GC-GNs/MTX, with ss-ctDNA as well as ds-ctDNA species.

### 3.2.2. Characterization by AFM

The AFM imaging can be used to map surface topography and structural properties of the solid surfaces modified by nanomaterials, and measure surface roughness [52]. The images related to surface morphological structures and line profiles obtained on the SPCE during step-by-step modification are presented in Fig. 4. The root-mean-square average of the surface roughness ($R_{rms}$) was 331 nm and 591 nm showing a growth of roughness during assembling of GNs on the SPCE surface (Table S1). While the attachment of MTX on SPCE-GNs surface via electrografting leads to a decrease of $R_{rms}$ by 27.6%, the loading of ss-ctDNA and ds-ctDNA on SPCE-GNs-MTX(ER) surface shows an increase of roughness from 428 to 549 and 748 nm, respectively. Furthermore, the line profiles corresponding to the AFM imaging could provide much-needed information about the height of the modified layers on the SPCE surface. The corresponding line profile of the SPCE electrode in Fig. 4A shows no fluctuations across the line, while the corresponding line profile of sticking GNs on the SPCE surface in Fig. 4B indicates a height of ~350 nm. The GNs-MTX presented on the line profile by red square marker (Fig. 4B) has a thickness of ~700 nm. The GNs layers are also observable on SPCE-GNs-MTX(ER) surface, which has been indicated by green triangle marker similar to that of Fig. 4B. Therefore, the thickness of the loaded MTX on the GNs is evaluated about 350 nm. The surface topography is expected to be same by adsorption of the ss-ctDNA or ds-ctDNA on SPCE-GNs-MTX(ER) electrode surface, which is demonstrated by their similar line profiles and heights (Fig. 4B-1 and 2). The AFM results further support formation of SPCE-GNs-MTX(ER) structure and adsorption of ctDNA on it.

### 3.2.3. Characterization by FESEM

The FESEM images of pristine GC, GC-GNs, GC-GNs-MTX(ER), GC-GNs-MTX(ER)-ss-ctDNA, and GC-GNs-MTX(ER)-ds-ctDNA surfaces are presented in Fig. 5. In comparison to bare electrode (Panel A′), the surface morphology of GC-GNs (Panel B′) is found to be completely different due to formation of the wrinkled GNs with layered structure. This special microstructure of GNs provides large surface area for adsorption of MTX, which has created irregularly-shaped spots marked by red circles (Panel B). A further FESEM study was performed to find out the

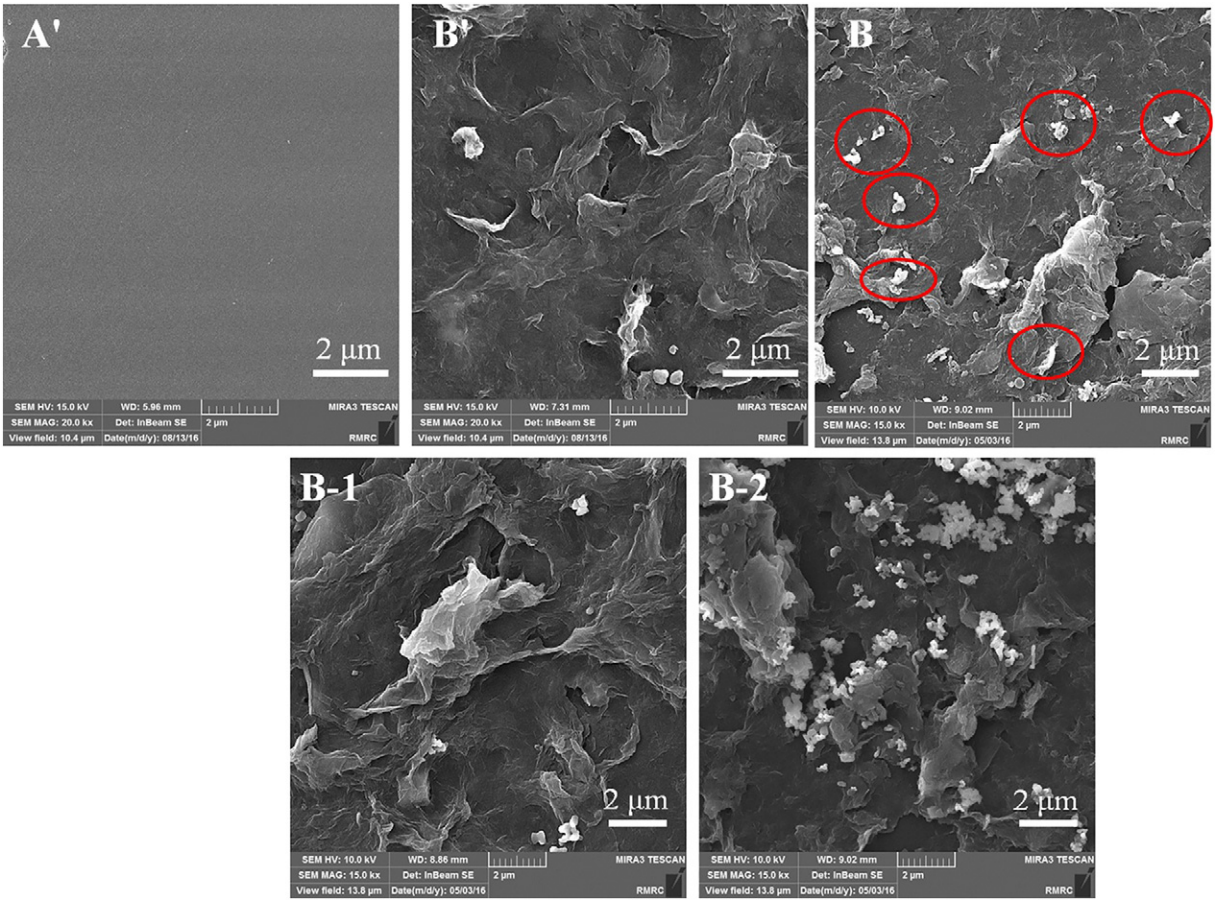


**Fig. 5.** The FESEM images obtained on (A′) GC, (B′) GC-GNs, (B) GC-GNs-MTX(ER), (B-1) GC-GNs-MTX(ER)-ss-ctDNA, and (B-2) GC-GNs-MTX(ER)-ds-ctDNA electrode surface.

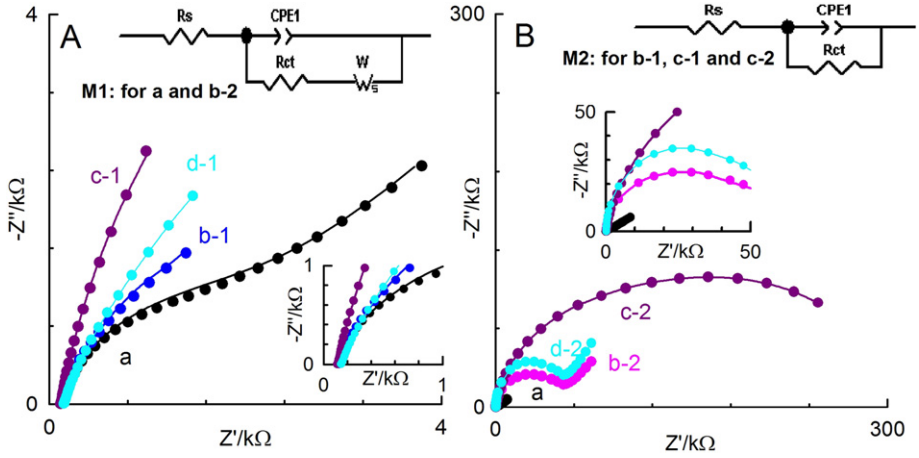


**Fig. 6.** (A) and (B) the EIS complex plane plots obtained in 0.1 M PBS, at pH 7.4, in the presence of 5.0 mM $[Fe(CN)_6]^{3-/4-}$ on (a) bare GC, (b-1) GC-GNs-MTX(ER), (c-1) GC-GNs-MTX(ER)-4T1, (d-1) GC-GNs-MTX(ER)-hFF, (b-2) GC-GNs/MTX, (c-2) GC-GNs/MTX-4T1, and (d-2) GC-GNs/MTX-hFF electrode systems at constant $E_{DC} = +0.200$ V (vs. SCE) and in a wide frequency range, from 10 kHz to 100 mHz, $E_{AC} = 5$ mV superimposed on $E_{DC}$. 4T1 stands for Mouse breast cancer cells 4T1 and hFF for Human foreskin fibroblast cells. MTX immobilized onto the GNs surface based on (A) covalent bonding via electrografting (ER) of MTX diazonium salt and (B) noncovalent bonding via electrostatic interactions of MTX. The EIS complex plane plots for expanded scale at high frequency (low impedance region) are also shown as insets.

interaction between GC-GNs-MTX(ER) and ctDNA. Loading ss-ctDNA or ds-ctDNA, respectively, indicate the growth of irregularly-shaped spots (Panels B-1 and 2), which might be happened due to adsorption of ctDNA onto GC-GNs-MTX(ER). Evidently, MTX plays an important role as a nucleation point to attach both of ss-ctDNA and ds-ctDNA, supporting high affinity of MTX in its immobilized form toward the DNAs.

### 3.3. Interaction of the systems with 4T1 mouse breast cancer cells

Interaction of GC-GNs-MTX(ER) and GC-GNs/MTX systems with 4T1 cancer cells is traced by using EIS [40]. The EIS is utilized as a direct, nondestructive, label-free, highly sensitive and efficient technique to follow biological interactions like capturing and detecting of the cancer cells [53]. The measurements are carried out in the presence of $[Fe(CN)_6]^{3-/4-}$ at $E_{DC} = +0.200$ V (vs. SCE) (Fig. 6A and B). The EIS data were fitted into appropriate equivalent circuit models (Fig. 6B, Insets), and the quantitative results for the model parameters were extracted (see Table 1 and its footnotes). The key parameters data are discussed in the following:

(i) The magnitude of double layer capacitance, $C_{dl}$, is proportional to the number of active sites on the surface, and the parameter "g" is related to the inhomogeneity of the sites and deformation in the semicircle of complex plane plot [2]. The $C_{dl}$ is decreased from GC-GNs (376 μF) to GC-GNs/MTX (0.43 μF) by a factor of (~99.8%). This effect can be explained based on neutralization of the surface charges, exposed by the GNs surface active sites, upon electrostatic adsorption of MTX on GC-GNs.

Alternatively, the $C_{dl}$ of GC-GNs (376 μF) modified by covalent adsorption of MTX via ER (218 μF) is changed by a factor of (~42%). This behavior could be due to highly *ordered structure of* GC-GNs-MTX(ER) allowing a large fraction of GC-GNs active sites being accessible after MTX adsorption (please follow the preparation of the systems, Supplementary data, Section 1).

(ii) The increase in the charge transfer resistance, $R_{ct}$, which is proportional to $1/k_{et}$ (the $k_{et}$ is the charge transfer rate constant of the redox probe), indicates closing of the surface against redox reaction of the probe. Variations in the $R_{ct}$ is resultant of several effects taking place in each step of modification, like hydrogen bonding, film thickness, and surface charges. The $R_{ct}$ is increased by a factor of ~4.5 and 5.3 upon incubation of GC-GNs-MTX(ER) and GC-GNs/MTX systems into separate solutions of 4T1 cells, respectively, supporting effective accumulation of these cells onto the surface of the systems. This behavior means that MTX, immobilized via *both* covalent and electrostatic bonds, conserves its affinity toward 4T1 cells, however, GC-GNs/MTX system loads (accumulates) more 4T1 cells compared with GC-GNs-MTX(ER) system.

(iii) To evaluate the selectivity of the constructed systems toward cancer cells, hFF cells, as a model of normal cells, are examined, in comparison with 4T1 cancer cells in the same conditions (Fig. 6, curves d-1 and d-2). Since the $R_{ct}$ is not significantly changed by this treatment, it can be concluded that hFF cells have not associated considerably with

**Table 1**
Electrochemical parameters extracted from the EIS data (Fig. 6), obtained on the GC electrode in different steps of the modification in 0.1 M PBS, pH 7.4, in the presence of 5.0 mM $[Fe(CN)_6]^{3-/4-}$ at $E_{DC} = +0.200$ V (vs. SCE).

| Electrode | $R_s(\Omega)$ | $R_{ct}(k\Omega)$ | $Q(10^{-6}\ s^g\ \Omega^{-1})$ | $C_{dl}(\mu F)$ | g | $k_{et}(cm\ s^{-1}) \times 10^{+4}$ |
|---|---|---|---|---|---|---|
| GC | 137 ± 2 | 4.2 ± 0.4 | 6.8 ± 0.2 | 2.6 ± 0.3 | 0.88 | 4.0 ± 0.4 |
| GC-GNs | 122 ± 0.2 | 16.5 ± 0.9 | 531 ± 6 | 376 ± 8 | 0.87 | 1.0 ± 0.1 |
| GC-GNs-MTX(ER) | 129 ± 1 | 3.8 ± 0.5 | 361 ± 8 | 218 ± 7 | 0.86 | 4.5 ± 0.5 |
| GC-GNs-MTX(ER)-4T1 | 145 ± 3 | 17 ± 2 | 389 ± 6 | 189 ± 6 | 0.80 | 0.10 ± 0.04 |
| GC-GNs-MTX(ER)-hFF | 131 ± 5 | 5.2 ± 0.6 | 375 ± 8 | 224 ± 6 | 0.85 | 3.2 ± 0.4 |
| GC-GNs/MTX | 213 ± 5 | 47 ± 5 | 0.52 ± 0.07 | 0.43 ± 0.02 | 0.98 | 0.039 ± 0.003 |
| GC-GNs/MTX-4T1 | 181 ± 4 | 249 ± 9 | 1.2 ± 0.1 | 0.42 ± 0.03 | 0.89 | 0.010 ± 0.008 |
| GC-GNs/MTX-hFF | 179 ± 3 | 59 ± 5 | 0.70 ± 0.07 | 0.42 ± 0.04 | 0.95 | 0.038 ± 0.005 |

$Q = C_{dl}^{g}\,[R_s^{-1} + R_{ct}^{-1}]^{1-g}$, where Q is related to the capacitance, $R_s$ and $R_{ct}$ are solution and charge transfer resistances. The "g" parameter is dimensionless related to the rotation of the complex plane plot, which in turn is connected to the electrode surface inhomogeneity, so that for ideal smooth electrodes g = 1. The $k_{et}$: charge transfer rate constant; $k_{et} = RT/n^2F^2R_{ct}CA$ for redox system in solution phase; n is number of transferred electron which is equal to one; C is concentration of redox probe; F is 96,500 C mole$^{-1}$ e$^{-1}$; R is gas constant 8.315 J mol$^{-1}$ K$^{-1}$ and T is Kelvin temperature. For clarity, GC-GNs plot is not presented in the panels.

the systems. This behavior clearly shows high affinity of the constructed systems for 4T1 cancer cells.

## 4. Conclusion

The methotrexate (MTX) anticancer drug was immobilized on GC-graphene surface via three methods; (a) EDC/NHS organic activators, (b) electrografting of diazonium salt and (c) noncovalent bonding, and then, the affinity of the immobilized MTX systems toward ss-ctDNA and ds-ctDNA was investigated for the first time. Electrochemical results together with surface analysis data, regarding physicochemical properties of the system, supported successful construction of the MTX-functionalized systems and their effective interaction with ctDNAs. The electrochemical results indicated that the amount of MTX immobilized on the graphene surface is affected by type of immobilization method, and a maximum amount of ($\Gamma_{MTX} = 9.3 \pm 0.9$ pmol cm$^{-2}$) was found via electrografting. Immobilized MTX showed high affinity for ctDNA in a wide dynamic range of concentrations. The nature of MTX and ctDNA interaction was of electrostatic and/or hydrogen bonding type, formed between O—H, N—H and C═O groups of MTX and different DNA functions. The graphene-modified-MTX systems were examined successfully for 4T1 cancer cells. This behavior opens a new physicochemical insight for therapy and drug delivery systems.

## Acknowledgment

The authors gratefully acknowledge the University of Isfahan for providing research facilities, the Iran National Science Foundation, Vise Presidency for Science and Technology (INSF/VPST) for the supports, and the INSF/VPST Iran High-Tech Laboratory Network (IH-TLN) for supporting the use of high technology facilities and services. Dr. Yousof Gheisari, Regenerative Medicine Lab, Isfahan University of Medical Sciences, is acknowledged for sharing his Lab facilities.

## Appendix A. Supplementary data

Supplementary data to this article can be found online at http://dx.doi.org/10.1016/j.bioelechem.2017.08.004.

## References

[1] E. Katz, I. Willner, Integrated nanoparticle-biomolecule hybrid systems: synthesis, properties, and applications, Angew. Chem. Int. Ed. 43 (2004) 6042–6108.
[2] R. Karimi Shervedani, Z. Akrami, H. Sabzyan, Nanostructure molecular assemblies constructed based on ex-situ and in-situ layer-by-layer ferrioxamation characterized by electrochemical and scanning tunneling microscopy methods, J. Phys. Chem. C 115 (2011) 8042–8055.
[3] M. Wanunu, A. Vaskevich, S.R. Cohen, H. Cohen, R. Arad-Yellin, A. Shanzer, I. Rubinstein, Branched coordination multilayers on gold, J. Am. Chem. Soc. 127 (2005) 17877–17887.
[4] K. Ulbrich, K. Holá, V. Šubr, A. Bakandritsos, J. Tuček, R. Zbořil, Targeted drug delivery with polymers and magnetic nanoparticles: covalent and noncovalent approaches, release control, and clinical studies, Chem. Rev. 116 (2016) 5338–5431.
[5] L. Zhang, J. Xia, Q. Zhao, L. Liu, Z. Zhang, Functional graphene oxide as a nanocarrier for controlled loading and targeted delivery of mixed anticancer drugs, Small 6 (2010) 537–544.
[6] J. Liu, L. Cui, D. Losic, Graphene and graphene oxide as new nanocarriers for drug delivery applications, Acta Biomater. 9 (2013) 9243–9257.
[7] W. Miao, G. Shim, S. Lee, S. Lee, Y.S. Choe, Y.K. Oh, Safety and tumor tissue accumulation of pegylated graphene oxide nanosheets for co-delivery of anticancer drug and photosensitizer, Biomaterials 34 (2013) 3402–3410.
[8] S.Q. Liu, N. Wiradharma, S.J. Gao, Y.W. Tong, Y.Y. Yang, Bio-functional micelles self-assembled from a folate-conjugated block copolymer for targeted intracellular delivery of anticancer drugs, Biomaterials 28 (2007) 1423–1433.
[9] B. Thierry, Drug nanocarriers and functional nanoparticles: applications in cancer therapy, Curr. Drug Deliv. 6 (2009) 391–403.
[10] A. Kumari, S.K. Yadav, S.C. Yadav, Biodegradable polymeric nanoparticles based drug delivery systems, Colloids Surf. B: Biointerfaces 75 (2010) 1–18.
[11] X. Yang, J.J. Grailer, S. Pilla, D.A. Steeber, S. Gong, Tumor-targeting, pH-responsive, stable unimolecular micelle as drug nanocarrier for targeted cancer therapy, Bioconjug. Chem. 21 (2010) 496–504.
[12] L.H. Hurley, DNA and its associated processes as targets for cancer therapy, Nat. Rev. Cancer 2 (2002) 188–200.
[13] X. Ling, W. Zhong, Q. Huang, K. Ni, Spectroscopic studies on the interaction of pazufloxacin with calf thymus DNA, J. Photochem. Photobiol. B Biol. 93 (2008) 172–176.
[14] M. Chauhan, K. Banerjee, F. Arjmand, DNA binding studies of novel copper(II) complexes containing L-tryptophan as chiral auxiliary: in vitro antitumor activity of Cu—Sn 2 complex in human neuroblastoma cells, Inorg. Chem. 46 (2007) 12032–12037.
[15] H. Mansouri-Torshizi, I. Mahboube, A. Divsalar, 2,2′-Bipyridinebutyldithiocarbamatoplatinum(II) and palladium(II) complexes: synthesis, characterization, cytotoxicity, and rich dna-binding studies, Bioorg. Med. Chem. 16 (2008) 9616–9625.
[16] Y. Temerk, M. Ibrahim, H. Ibrahim, M. Kotb, Interactions of an anticancer drug formestane with single and double stranded DNA at physiological conditions, J. Photochem. Photobiol. B Biol. 149 (2015) 27–36.
[17] K. Prabakaran, S. Rajeswari, Spectroscopic investigations on the synthesis of nano-hydroxyapatite from calcined egg shell by hydrothermal method using cationic surfactant as template, Spectrochim. Acta A 74 (2009) 1127–1134.
[18] W. Zhong, J.-S. Yu, Y. Liang, Chlorobenzylidine–herring sperm DNA interaction: binding mode and thermodynamic studies, Spectrochim. Acta A 59 (2003) 1281–1288.
[19] K. Sandstrom, S. Warmlander, M. Leijon, A. Graslund, H-1 NMR studies of selective interactions of norfloxacin with double-stranded DNA, Biochem. Biophys. Res. Commun. 304 (2003) 55–59.
[20] J. Kang, Z. Li, X. Lu, Electrochemical study on the behavior of morin and its interaction with DNA, J. Electroanal. Chem. 40 (2006) 1166–1171.
[21] M. Song, R. Zhang, X. Wang, Nano-titanium dioxide enhanced biosensing of the interaction of dacarbazine with DNA and DNA bases, Mater. Lett. 60 (2006) 2143–2147.
[22] S.S. Kalanur, U. Katrahalli, J. Seetharamappa, Electrochemical studies and spectroscopic investigations on the interaction of an anticancer drug with DNA and their analytical applications, J. Electroanal. Chem. 636 (2009) 93–100.
[23] J. Wang, M. Ozsoz, X. Cai, G. Rivas, H. Shiraishi, D.H. Grant, M. Chicharro, J. Fernandes, E. Paleček, Interactions of antitumor drug daunomycin with DNA in solution and at the surface, Bioelectrochem. Bioenerg. 45 (1998) 33–40.
[24] D. Rawtani, Y.K. Agrawal, Interaction of methotrexate with DNA using gold nanoparticles as a probe, Instrum. Sci. Technol. 42 (2014) 308–319.
[25] Y. Pan, N.G. Sahoo, L. Li, The application of graphene oxide in drug delivery, Expert Opin. Drug Deliv. 9 (2012) 1365–1376.
[26] Y.-H. Chen, C.-Y. Tsai, P.-Y. Huang, M.-Y. Chang, P.-C. Cheng, C.-H. Chou, Methotrexate conjugated to gold nanoparticles inhibits tumor growth in a syngeneic lungtumor model, Mol. Pharm. 4 (2007) 713–722.
[27] C. Chittasupho, M. Jaturanpinyo, S. Mangmool, Pectin nanoparticle enhances cytotoxicity of methotrexate against HepG2 cells, Drug Deliv. 20 (2013) 1–9.
[28] T. Muthukumar, S. Prabhavathi, M. Chamundeeswari, T.P. Sastry, Bio-modified carbon nanoparticles loaded with methotrexate possible carrier for anticancer drug delivery, Mater. Sci. Eng. C 36 (2014) 14–19.
[29] E. Corem-Salkmon, Z. Ram, D. Daniels, B. Perlstein, D. Last, S. Salomon, G. Tamar, R. Shneor, D. Guez, S. Margel, Y. Mardor, Convection-enhanced delivery of methotrexate-loaded maghemite nanoparticles, Int. J. Nanomedicine 6 (2011) 1595–1602.
[30] V. Georgakilas, M. Otyepka, A.B. Bourlinos, V. Chandra, N. Kim, K.C. Kemp, P. Hobza, R. Zboril, K.S. Kim, Functionalization of graphene: covalent and non-covalent approaches, derivatives and applications, Chem. Rev. 112 (2012) 6156–6214.
[31] L. Bai, D. Zhao, Y. Xu, J. Zhang, Y. Gao, L. Zhao, Inductive heating property of graphene oxide–$Fe_3O_4$ nanoparticles hybrid in an AC magnetic field for localized hyperthermia, Mater. Lett. 68 (2012) 399–401.
[32] Z. Liu, J.T. Robinson, X. Sun, H. Dai, PEGylated nano-graphene oxide for delivery of water insoluble cancer drugs, J. Am. Chem. Soc. 130 (2008) 10876–10877.
[33] V. Georgakilas, J.N. Tiwari, K.C. Kemp, J.A. Perman, A.B. Bourlinos, K.S. Kim, R. Zboril, Noncovalent functionalization of graphene and graphene oxide for energy materials, biosensing, catalytic, and biomedical applications, Chem. Rev. 116 (2016) 5464–5519.
[34] W. Zhang, Z. Guo, D. Huang, Z. Liu, X. Guo, H. Zhong, Synergistic effect of chemo-photothermal therapy using PEGylated graphene oxide, Biomaterials 32 (2011) 8555–8561.
[35] Y. Wang, H. Liu, F. Wang, Y. Gao, Electrochemical oxidation behavior of methotrexate at DNA/SWCNT/Nafion composite film-modified glassy carbon electrode, J. Solid State Electrochem. 16 (2012) 3227–3235.
[36] F. Wang, Y. Wu, J. Liu, B. Ye, DNA Langmuir–blodgett modified glassy carbon electrode as voltammetric sensor for determinate of methotrexate, Electrochim. Acta 54 (2009) 1408–1413.
[37] H. Zhou, Q. Shen, S. Zhang, B. Ye, Combination of methotrexate and emodin interacting with DNA, Anal. Lett. 42 (2009) 1418–1429.
[38] B. Rafique, A.M. Khalid, K. Akhtar, A. Jabbar, Interaction of anticancer drug methotrexate with DNA analyzed by electrochemical and spectroscopic methods, Biosens. Bioelectron. 44 (2013) 21–26.
[39] M. Wojtoniszak, K. Urbas, M. Peruzyńska, M. Kurzawski, M. Droździk, E. Mijowska, Covalent conjugation of graphene oxide with methotrexate and its antitumor activity, Chem. Phys. Lett. 568–569 (2013) 151–156.
[40] R. Karimi Shervedani, F. Yaghoobi, M. Torabi, M. Samiei Foroushani, Nanobioconjugated system formed of folic acid—deferrioxamine—Ga(III) on gold surface: preparation, characterization, and activities for capturing of mouse breast cancer cells 4T1, J. Phys. Chem. C 120 (2016) 23212–23220.
[41] A. Nabok, A. Tsargorodskaya, D. Gauthier, F. Davis, S.P.J. Higson, T. Berzina, L. Cristofolini, M.P. Fontana, Hybridization of genomic DNA adsorbed electrostatically onto cationic surfaces, J. Phys. Chem. B 113 (2009) 7897–7902.

[42] W.S. Hummers, R.E. Offeman, Preparation of graphitic oxide, J. Am. Chem. Soc. 80 (1958) 1339.
[43] R. Karimi Shervedani, A. Amini, Sulfur-doped graphene as a catalyst support: influences of carbon black and ruthenium nanoparticles on the hydrogen evolution reaction performance, Carbon 93 (2015) 762–773.
[44] R. Karimi Shervedani, E. Ansarifar, M. Foroushani, Electrocatalytic activities of graphene/nile blue nanocomposite toward determination of hydrogen peroxide and nitrite ion, Electroanalysis 28 (2016) 1957–1969.
[45] A.D.R. Pontinha, S.M.A. Jorge, V.C. Diculescu, M. Vivan, A.M. Oliveira-Brett, Antineoplasic drug methotrexate redox mechanism using a glassy carbon electrode, Electroanalysis 24 (2012) 917–923.
[46] D. Samanta, A. Sarkar, Immobilization of bio-macromolecules on self-assembled monolayers: methods and sensor applications, Chem. Soc. Rev. 40 (2011) 2567–2592.
[47] N.A. Elmarzugi, T. Adali, A.M. Bentaleb, E.I. Keleb, A.T. Mohamed, A.M. Hamza, Spectroscopic characterization of PEG-DNA biocomplexes by FTIR, J. Appl. Pharm. Sci. 4 (2014) 6–10.
[48] R. Karimi Shervedani, S. Pourbeyram, Electrochemical determination of calf thymus DNA on Zr(IV) immobilized on gold-mercaptopropionic-acid self-assembled monolayer, Bioelectrochemistry 77 (2010) 100–105.
[49] B. Yang, Z. Liu, Z. Guo, W. Zhang, M. Wan, X. Qin, H. Zhong, In situ green synthesis of silver-graphene oxide nanocomposites by using tryptophan as a reducing and stabilizing agent and their application in SERS, Appl. Surf. Sci. 316 (2014) 22–27.
[50] R.M. Silverstein, G.C. Bassler, T.C. Morrill, Spectrometric Identification of Organic Compounds, 4th ed. John Wiley and Sons, New York, 1981.
[51] B.-X. Ye, L.-J. Yuan, C. Chen, J.-C. Tao, Electrochemical and spectroscopic study of the interaction of indirubin with DNA, Electroanalysis 17 (2005) 1523–1528.
[52] P. Eaton, P. West, Atomic Force Microscopy, Oxford University Press, 2010.
[53] A. Venkatanarayanan, T.E. Keyes, R.J. Forster, Label-free impedance detection of cancer cells, Anal. Chem. 85 (2013) 2216–2222.